On the "Tertiary Structure" of Poly-Carbenes; Self-Assembly of sp(3)-Carbon-Based Polymers into Liquid-Crystalline Aggregates

12 AUTHORS, INCLUDING:

Theo Dingemans
Delft University of Technology
106 PUBLICATIONS **1,505** CITATIONS

SEE PROFILE

Johannes A A W Elemans
Radboud University Nijmegen
126 PUBLICATIONS **4,520** CITATIONS

SEE PROFILE

Joost N H Reek
University of Amsterdam
386 PUBLICATIONS **10,791** CITATIONS

SEE PROFILE

Bas de Bruin
University of Amsterdam
228 PUBLICATIONS **3,997** CITATIONS

SEE PROFILE

On the "Tertiary Structure" of Poly-Carbenes; Self-Assembly of sp³-Carbon-Based Polymers into Liquid-Crystalline Aggregates

Nicole M. G. Franssen,[a, b] **Bernd Ensing,**[a] **Maruti Hegde,**[c] **Theo J. Dingemans,**[c] **Ben Norder,**[d] **Stephen J. Picken,**[d] **Gert O. R. Alberda van Ekenstein,**[e] **Ernst R. H. van Eck,**[f] **Johannes A. A. W. Elemans,**[f] **Mark Vis,**[g] **Joost N. H. Reek,**[a] and **Bas de Bruin***[a]

Abstract: The self-assembly of poly-(ethylidene acetate) (*st*-PEA) into van der Waals-stabilized liquid-crystalline (LC) aggregates is reported. The LC behavior of these materials is unexpected, and unusual for flexible sp³-carbon backbone polymers. Although the dense packing of polar ester functionalities along the carbon backbone of *st*-PEA could perhaps be expected to lead directly to rigid-rod behavior, molecular modeling reveals that individual *st*-PEA chains are actually highly flexible and should not reveal rigid-rod induced LC behavior. Nonetheless, *st*-PEA clearly reveals LC behavior, both in solution and in the melt over a broad elevated temperature range. A combined set of experimental measurements, supported by MM/MD studies, suggests that the observed LC behavior is due to self-aggregation of *st*-PEA into higher-order aggregates. According to MM/MD modeling *st*-PEA single helices adopt a flexible helical structure with a preferred *trans-gauche syn-syn-anti-anti* orientation. Unexpectedly, similar modeling experiments suggest that three of these helices can self-assemble into triple-helical aggregates. Higher-order assemblies were not observed in the MM/MD simulations, suggesting that the triple helix is the most stable aggregate configuration. DLS data confirmed the aggregation of *st*-PEA into higher-order structures, and suggest the formation of rod-like particles. The dimensions derived from these light-scattering experiments correspond with *st*-PEA triple-helix formation. Langmuir–Blodgett surface pressure–area isotherms also point to the formation of rod-like *st*-PEA aggregates with similar dimensions as *st*-PEA triple helixes. Upon increasing the *st*-PEA concentration, the viscosity of the polymer solution increases strongly, and at concentrations above 20 wt% *st*-PEA forms an organogel. STM on this gel reveals the formation of helical aggregates on the graphite surface–solution interface with shapes and dimensions matching *st*-PEA triple helices, in good agreement with the structures proposed by molecular modeling. X-ray diffraction, WAXS, SAXS and solid state NMR spectroscopy studies suggest that *st*-PEA triple helices are also present in the solid state, up to temperatures well above the melting point of *st*-PEA. Formation of higher-order aggregates explains the observed LC behavior of *st*-PEA, emphasizing the importance of the "tertiary structure" of synthetic polymers on their material properties.

Keywords: liquid crystals · polymers · sp³ backbone · supramolecular aggregates · triple helix

[a] Dr. N. M. G. Franssen, Dr. B. Ensing, Prof. Dr. J. N. H. Reek, Prof. Dr. B. de Bruin
Van 't Hoff Institute for Molecular Sciences (HIMS)
Universiteit van Amsterdam, P. O. Box 94720
1090 GS Amsterdam (The Netherlands)
E-mail: b.debruin@uva.nl

[b] Dr. N. M. G. Franssen
Dutch Polymer Institute DPI, P. O. Box 902
5600 AX Eindhoven (The Netherlands)

[c] M. Hegde, Prof. Dr. T. J. Dingemans
Faculty of Aerospace Engineering, Delft University of Technology
Kluyverweg 1, 2629 HS Delft (The Netherlands)

[d] B. Norder, Prof. Dr. S. J. Picken
Department of Chemical Engineering, Faculty of Applied Sciences
Delft University of Technology, Julianalaan 136
2628 BL, Delft (The Netherlands)

[e] G. O. R. Alberda van Ekenstein
Zernike Institute for Advanced Materials
Rijksuniversiteit Groningen, Nijenborgh 4
9747 AG Groningen (The Netherlands)

[f] Dr. E. R. H. van Eck, Dr. J. A. A. W. Elemans
Radboud Universiteit Nijmegen
Institute for Molecules and Materials, Heyendaalseweg 135
6525 AJ Nijmegen (The Netherlands)

[g] M. Vis
Van 't Hoff Laboratory for Physical and Colloid Chemistry
Debye Institute for Nanomaterials Science, Universiteit Utrecht
Padualaan 8, 3584 CH Utrecht (The Netherlands)

💻 Supporting information for this article is available on the WWW under http://dx.doi.org/10.1002/chem.201301403.

Introduction

In nature, macromolecules (RNA, DNA and polypeptides, such as proteins) have evolved towards serving certain purposes, and their desired properties (e.g., rigidity or specific recognition of other molecules) are mainly dictated by the complex secondary and tertiary structures they adopt. An important class of tertiary structures is formed by helical assemblies, which are ubiquitously found in nature and are responsible for the most important biological functions.[1] The most well-known example of a helical assembly is DNA, which forms a double helix, and its structure is intricately linked to its biological function. As such, the properties and biological behavior of DNA are completely different from that of RNA, which is a single-stranded DNA analogue and does not form a long double helical tertiary structure on its own. RNA or other synthetic oligonucleotides can form assemblies upon selectively binding with double-stranded DNA target sequences, which results in the formation of a triple helix.[2,3] Formation of these specific macromolecular assemblies has been proposed as a suitable approach for selective gene expression/repression and DNA repair (for a review, see ref. [4]). Another example of a helical assembly in biological systems is collagen, which possesses a great tensile strength due to its assembly into triple-helix fibers, and is as such perfectly designed to provide support and stability to tissue.[5]

Although it is a common feature for biological macromolecules to assemble into helical tertiary structures or bundles, helical assembly of synthetic macromolecules is unusual.[1] Recent advances in the field of supramolecular chemistry have led to the synthesis of a limited number of synthetic macromolecules that form, under specific conditions, a double helix structure (for examples, see reviews by Nolte,[6,7] Furusho[1] and Yashima[8]). Formation of higher-order assemblies from synthetic, high molecular-weight polymers is, however, still extremely rare. Some reports dealing with formation of triple-stranded metal-bound helicates have been published in recent years (for examples, see a review by Yashima[8]), as well as reports describing the helical structure adapted by stereocomplex polymethylmethacrylate (PMMA), which adopts a triple-helix-like structure through supramolecular assembly of two isotactic strands and one syndiotactic strand (Figure 1).[9]
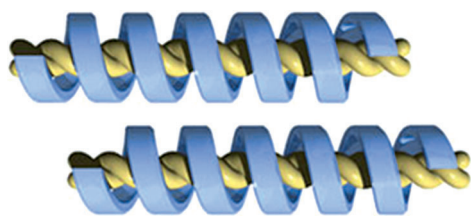

Figure 1. Schematic representation of the triple-helix-like structure of stereocomplex PMMA: a double helix formed by two strands of *it*-PMMA (yellow) surrounded by a single strand of *st*-PMMA (blue). (Reproduced from ref. [10] with permission from the American Chemical Society; copyright 2008.)

Formally this structure should be considered as an inclusion complex, in which a double helix formed by two strands of isotactic PMMA is surrounded by a strand of syndiotactic PMMA.[1] Due to its specific triple-helix-like structure, stereocomplex PMMA reveals very different properties than atactic or syndiotactic PMMA and exhibits, among others, enhanced thermal stability compared to the different structures of (proposed double helix) homo-assemblies formed by either syndiotactic PMMA or isotactic PMMA. As a result, stereocomplex PMMA has found its way into advanced applications, such as ultrathin films and thermoplastic elastomers.[11,12] This emphasizes that supramolecular assembly of synthetic macromolecules into a more complex helical aggregate drastically changes the polymer properties, and can lead to the development of a completely new class of materials with unique functions stemming from their "tertiary structure", in analogy with the above-described biomolecules.

The formation of synthetic helical assemblies might well play an important role in the development of new liquid-crystalline polymers (LCPs). LCPs are of growing importance because of their potential applications, such as actuators and in the field of organic photovoltaic materials. LCPs generally contain segments constructed from sp^2-hybridized carbon atoms, in order to provide sufficient rigidity to the macromolecular chains to allow the formation of a liquid-crystalline phase. Rigidity could, in principle, also be induced by the formation of helical assemblies that lock the polymer chains in a specific, rigid conformation. This would eliminate the need for sp^2-hybridization and potentially allows the formation of LCPs from sp^3-based polymers, such as polyolefins, which has up to now only been achieved with very limited success. Only few examples exist dealing with LC properties of linear polyolefin-like carbon-chain materials, and their LC phases are only observed under rather extreme conditions.[13–15] The above-described helical PMMA assemblies (including stereocomplex PMMA) do not give rise to the formation of LC phases.

We have already demonstrated that syndiotactic carbene polymers containing a fully sp^3-based backbone structure exhibit both lyotropic and thermotropic liquid crystalline behavior with nematic stability over a broad temperature range[17a] (Figure 2; for an overview of the field of carbene polymers, see refs. [16–18]). To our knowledge, this is the first example of a stable fully sp^3-based, main-chain liquid crystalline polymer. We thus far assumed that the rigidity in these polymers is induced by the presence of rather bulky side groups at every single carbon atom of the polymer backbone, thus preventing free rotation around the C−C bonds in the backbone and locking the polymers in a rigid helical conformation (i.e., rigid-rod behavior of the single chains). Analogous atactic polymers made by radical polymerization of difunctionalized olefins are obtained as sticky oils and exhibit thermotropic LC properties only under shear, indicating that the stereoregularity of the carbene polymers plays an important role.[19] Hence, this new class of *stereoregular* carbene polymers exhibits material properties
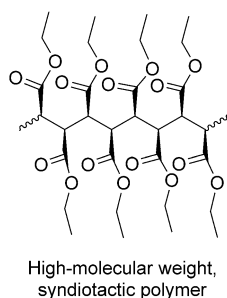
FULL PAPER

Figure 2. Example of a liquid crystalline carbene polymer (syndiotactic poly(ethylidene acetate); *st*-PEA) with a fully sp³-based backbone as obtained by Rh-mediated carbene polymerization using a diazoester as carbene monomer precursor.

Figure 3. The realm of main-chain sp³-carbon based polymers, showing the well-known amorphous and semi-crystalline morphologies on the right and the new liquid crystalline morphologies on the left.

very different from other existing polymers, such as poly-(meth)acrylates, as a result of the densely packed *and* stereoregularly-placed functionalities.

Observation of liquid-crystalline behavior of carbene polymers provides unique possibilities for the formation of highly (macroscopically) aligned fibers and films of fully sp³-based polymers, which have been inaccessible up to now due to the absence of other stable sp³-based LCPs. These aligned structures are expected to reveal novel material properties, possibly opening up new application areas both from a structural and functional point of view.

To fully exploit the potential of these sp³-based LCPs it is necessary to study their 3D structure and their potential to assemble into more complex supramolecular aggregates ("tertiary structure") in more detail. The highly syndiotactic carbene polymers that can be obtained in a controlled way by Rh-mediated carbene polymerization provide an excellent starting point for such studies.[17] Recently, the structure of such polymers containing alkyl side chains ranging from C6 to C18 have been reported to form highly ordered hexagonal columnar phases whereas formation of supramolecular aggregates was not observed.[20] Surprisingly, shortening the alkyl chain to C2 (i.e., poly(ethylidene)acetate, *st*-PEA; Figure 2) leads to a completely different behavior. This polymer forms a nematic LC phase, although its phase structure is thus far poorly understood. Since the molecular weight of *st*-PEA can easily be tuned by varying the reaction conditions, we set out to study the above-mentioned polymer properties of *st*-PEA in order to find an explanation for its different behavior.

Here we present our combined experimental and computational efforts aiming at understanding the LC behavior of *st*-PEA. The combined information from molecular mechanics-based molecular dynamic studies (MM/MD), scanning tunneling microscopy (STM), Langmuir–Blodgett surface pressure–area isotherms, WAXS, SAXS and X-ray diffraction studies, DSC, polarized microscopy and solid state NMR spectroscopy strongly suggests that *st*-PEA helices self-assemble into higher-order van der Waals-stabilized triple-helix aggregates, thus explaining the observed polymer properties. Formation of nematic phases by polymer self-assembly uncovers a thus far unexplored new area in
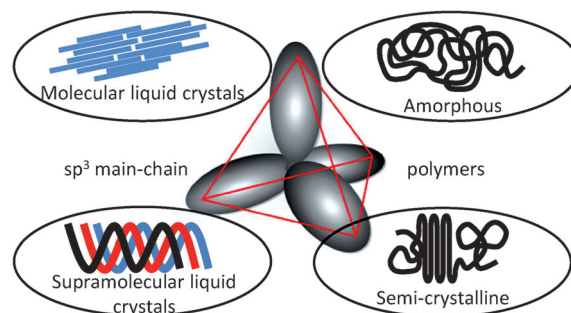
the realm of sp³-carbon-based polymers and is expected to broaden their application window tremendously (Figure 3).

Results and Discussion

Modeled structure of *st*-PEA: We first focused on molecular modeling techniques to gain information about the flexibility/stiffness of *st*-PEA in order to understand the possible rigid-rod behavior of this polymer in relation to its LC behavior. This led to rather surprising results. Finding the (global) minimum energy structure of a short *st*-PEA oligomer by straightforward molecular mechanics (MM) optimization is hampered by the rather rugged potential energy surface of these molecules. We, therefore, also performed a series of short classical molecular dynamics (MD) simulations of *st*-PEA fragments in the gas phase at temperatures ranging from 5 to 300 K. The simulations employ a DFT-calibrated version of the Amber force field and were started from different molecular geometries, setup and optimized with a molecule builder program. In particular, the initial configurations sampled different carbon backbone dihedral angles and side-chain orientations as defined by their H−C−C=O dihedral angles (Figure 4). Both the MM optimi-
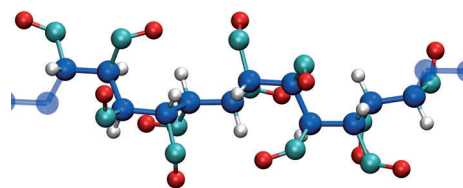

Figure 4. Detailed representation of the backbone conformation showing the *trans-gauche* conformation and the *syn-syn-anti-anti* H−C−C=O torsions (OEt moieties of the ester groups are omitted for clarity).

zations and the MD simulations show that the *st*-PEA chain assumes a helical configuration to minimize the steric repulsion between the C(O)OEt side chains present at every single backbone carbon atom (Figure 4 and Figure 5). This behavior is somewhat related to the helical folding of *st*-PMMA.[21] Of the structures found for a short *st*-PEA model
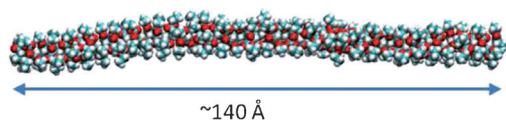
Figure 5. Snapshot from a molecular dynamics simulation at $T = 5$ K of a *st*-PEA fragment composed of 128 CHC(O)OEt units, showing the formation of a *trans-gauche* helix and the favorable arrangement of the C=O fragments.

Figure 7. Snapshot from a molecular dynamics simulation at $T = 5$ K of a *st*-PEA fragment composed of 128 CHC(O)OEt units, showing the formation of a more compact flexible helix with a more random conformation of the HC−C=O torsions (top).

fragment of 128 backbone units, a *trans-gauche* helix (secondary structure) is the most stable configurational state, in which the backbone dihedral angles are alternating close to $-45°$ and $175°$ in the left-handed (*M*) helix or with the opposite signs in the right-handed (*P*) helix. As expected, *st*-PEA has no preferred handedness. Interestingly, the side chain orientations assume a *syn-syn-anti-anti* pattern at very low temperatures. However, the rotational barrier is rather small, and at room temperature, the side chain configurations are more disordered (Figure 6).

Another helical structure that we found is shown in Figure 7. This structure has a smaller helical pitch and is thus thicker and shorter than the *trans-gauss* helix, but is also about 3 kT (1.8 kcal mol^{-1}) per monomer higher in energy. To our surprise, the simulations at $T = 300$ K revealed that both the *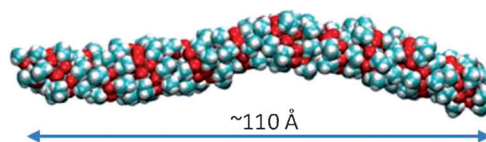trans-gauche* chain and the more compact chain are much more flexible than anticipated (Figure 8). In fact, they are so flexible that they cannot be regarded as rigid rods at all, and thus cannot be responsible for the experimentally observed LC behavior (vide infra). As the rigid-rod behavior of *st*-PEA cannot be understood
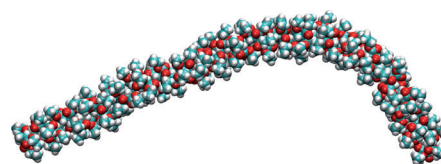

Figure 8. Snapshot from a molecular dynamics simulation at $T = 300$ K of a *syn-syn-anti-anti st*-PEA fragment composed of 128 CHC(O)OEt units, emphasizing its flexibility.
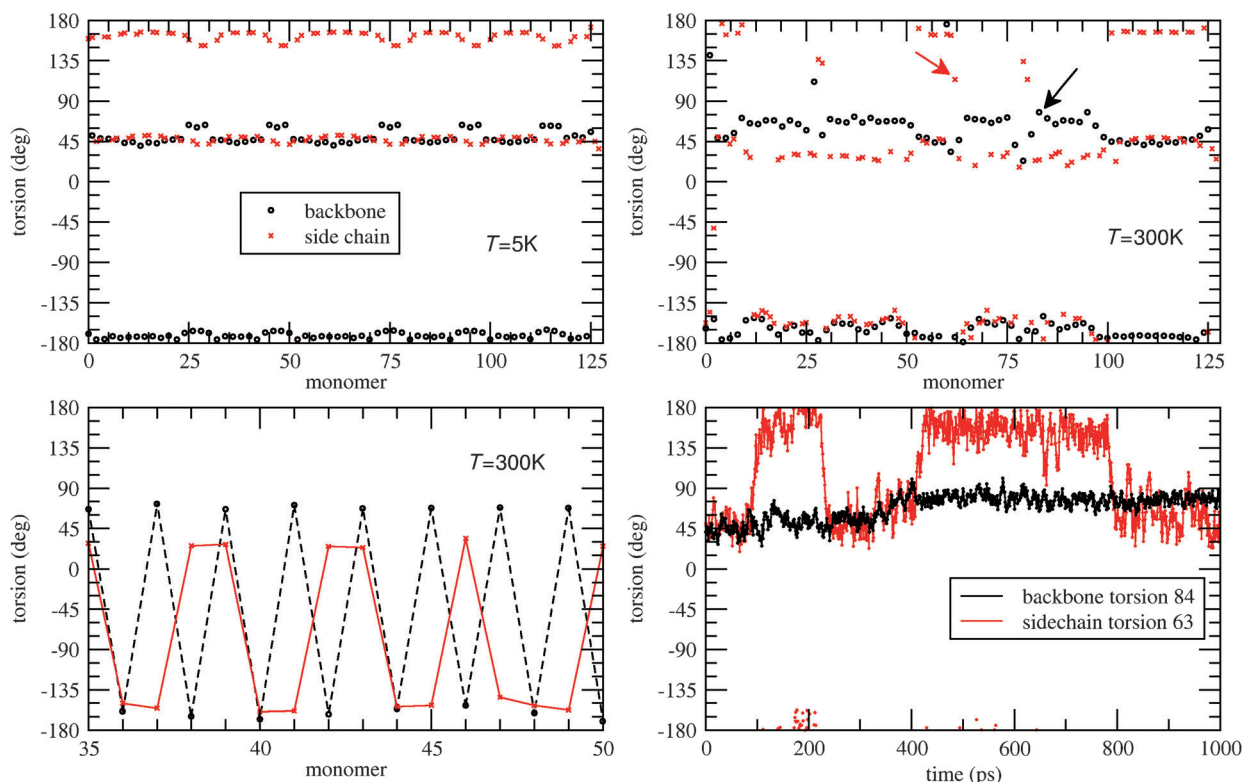

Figure 6. Values for the H−C−C=O torsion angles (grey) and C−C torsion angles of the polymer backbone (black) of a left-handed helix as a function of the position in the polymer fragment, showing the *syn-syn-anti-anti* conformation for the H−C−C=O torsions and the *trans-gauche* conformation of the backbone at 5 K (top left) and 300 K (top right and bottom left). The bottom-right picture shows the time profile of one H−C−C=O torsion and one C−C torsion at 300 K, revealing that rotation around the H−C−C=O torsion is possible.

from regarding the isolated chain, we moved on to model the behavior of small assemblies of *st*-PEA chains.

MD simulations of three of the 128-monomer *st*-PEA helical chains stacked in a parallel configuration show a very remarkable behavior. The stacked helices spontaneously self-assemble in a supramolecular way to form a rigid, rod-like super helix ("tertiary structure"), provided that the single helices have the same handedness (Figure 9).
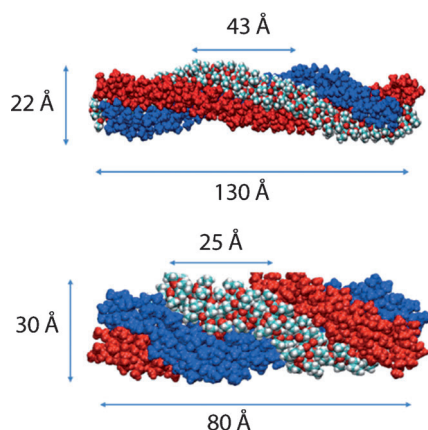

Figure 9. Snapshot from a molecular dynamics simulation at $T = 300$ K of three right-handed *st*-PEA fragments composed of 128 CHC(O)OEt units revealing the formation of right-handed triple-helix assemblies for the structured *syn-syn-anti-anti* single helices (top), and the more random helices (bottom) showing the different dimensions. The chains are identical but are represented in different colors for clarity.

The resulting triple helix has the same handedness as the single helices of which it is composed. When a mixture of two *M*-helices and one *P*-helix (or the opposite) was allowed to equilibrate, formation of a triple helix was not observed. Also, attempts to obtain triple helices exhibiting the opposite handedness of that of the single helices were unsuccessful: upon applying a torsion potential the triple helix can be rotated in the opposite direction, but the triple helix immediately unfolded upon release of this potential, in order to equilibrate to a triple helix with the same handedness as the single helices.

The top panel in Figure 9 shows a snapshot from the 1 ns simulation at $T = 300$ K starting from three of the *trans-gauss M* chains (Figure 4 and Figure 5), in which the triple helix is formed with a pitch of 130 Å and a top–top longitudinal interchain distance of the three single helices of about 43 Å. Starting from three single *M*-helices in the more compact and energetically less favorable configuration (Figure 7) leads to a shorter triple helix that has a pitch of 80 Å and a top–top longitudinal interchain distance of approximately 25 Å between the single helices (Figure 9, bottom panel). The average potential energy difference between these stretched and more compact triple-helix assemblies at $T = 300$ K is with approximately 1 kcal $mol^{-1} monomer^{-1}$ somewhat smaller than the difference between the single chains. Based on this (still significant) energy difference we expect the stretched triple helix to be

predominant in the melt and in solution with a rather inert solvent, such as chloroform. We believe, however, that the more compact helix conformation can play an important role under certain experimental conditions, for example, through interaction with a surface in STM experiments, as we will discuss in the following section.

Noteworthy, these triple helices are held together solely by interchain van der Waals interactions between the ethyl fragments of the different single-helix chains. Since the C=O fragments are "hidden" in the interior of the single helices, contribution of dipole interactions to the stability of the triple helix is only marginal (less than one third of the total interactions). When four single helices are allowed to equilibrate in the MD/MM simulations, a triple helix with a "loose end" is observed, which is the onset for the formation of a network of triple helices in which single helices interconnect two or more triple helices (Figure 10) leading to the formation of physical crosslinks (Figure 11). Formation of
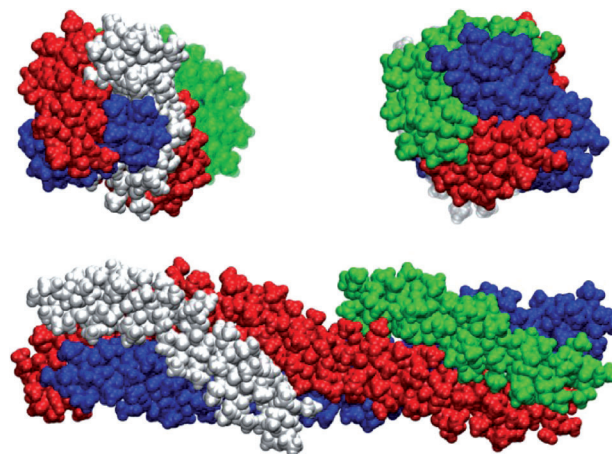

Figure 10. Schematic representation of the formation of physical crosslinks by interconnecting single helices. Front view, showing a triple helix formed by the red, blue and white single helices whereas the shorter green helix is not participating (top left), side view showing the chain ends of the shorter white and green helices (bottom) and back view, showing a triple helix formed by the red, blue and green single helices whereas the shorter white helix is not participating (top right). The single-helix chains are identical but represented in different colors for clarity.

higher-order helices (e.g., quadruple helices) does not occur according to these simulations, indicating that the triple-helix structure is the most stable assembly. Formation of synthetic sp³-based helical assemblies stabilized by van der Waals interactions are rare, and it has only been observed for formation of the (double-) helical assemblies of PMMA[1] described in the introduction, as well as for poly-(ethyleneimine) double helices and co-polymers thereof.[22]

Most literature examples of naturally occurring and bio-inspired higher-order helical assemblies exhibit much stronger interstrand interactions, such as hydrogen bonds or metal–ligand interactions, between the macromolecules that are responsible for the formation of the helical assemblies.
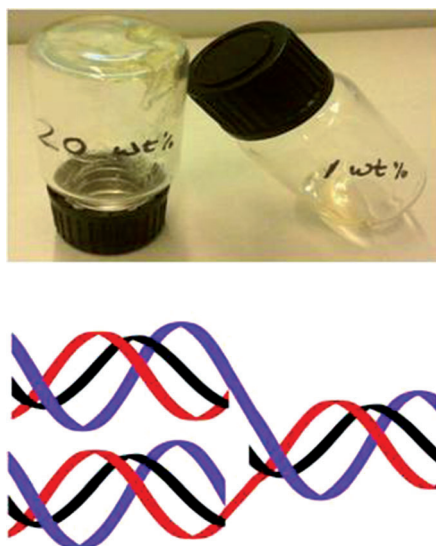
Figure 11. Pictures of a solution of *st*-PEA at a concentration of 1 wt % in CHCl₃ and of a stiff polymer gel at 20 wt % *st*-PEA in CHCl₃ (top). This gel is likely the result of physical crosslinks formed by single helix chains (depicted as black, red and purple ribbons) assembling into interconnected triple helices (bottom).

Such interactions, which repeatedly occur between specific segments of the resulting macromolecular chain-array, also explain the stability of these abundant assemblies. For the collagen triple helix, for example, interstrand hydrogen bonds are observed once per three amino acid units in the backbone, and each hydrogen bond accounts for helix stabilization by about 2 kcal mol^{-1}.[23] Some synthetic triple-stranded helicates gain stability from abundant metal–ligand interactions, and their shape is directed by both the ligand structures and the coordination geometries of the metal centers.[8] The *st*-PEA triple helix shown in Figure 9 does not contain any of these stronger electrostatic interactions between the three *st*-PEA chains of which it is composed, but is a rare example of a van der Waals-stabilized triple helix. Stereocomplex PMMA is the only other example of such a van der Waals-stabilized higher-order assembly we are aware of, but this assembly is composed of two different polymers (*st*-PMMA and *it*-PMMA) in a 2:1 ratio. The *st*-PEA triple helix shown in Figure 9 seems to be the first van der Waals-stabilized triple helix composed of three identical polymer chains.

Experimental proof for self-assembly of *st*-PEA: Several experiments confirm that *st*-PEA self-assembles into higher-order aggregates, and the combined information gathered from scanning tunneling microscopy (STM), Langmuir–Blodgett surface pressure–area isotherms, X-ray diffraction studies and solid state NMR spectroscopy studies suggests that *st*-PEA indeed self-assembles into van der Waals-stabilized triple-helical aggregates under the experimental conditions in solution, in the solid state, and in the melt, in which *st*-PEA adopts a similar "tertiary structure" as found in the MM/MD simulations.

Self-assembly of *st*-PEA in solution and *st*-PEA aggregate detection on a graphite surface with STM: The aggregation behavior of *st*-PEA in solution depends on its concentration. Dynamic light scattering (DLS) experiments confirmed the presence of rigid, rod-like particles with dimensions similar to those of the MM/MD modeled *st*-PEA triple helix ($M_w = 120$ kDa, PDI 2.9) at concentrations ≥ 1 wt % in chloroform (see Figures S1 and S2 in the Supporting Information for more details). The presence of such structures was not observed at lower concentrations, indicating that *st*-PEA is most likely present as single helices at these concentrations. These results confirm that *st*-PEA chains self-assemble into higher-order rod-like aggregates upon increasing the *st*-PEA concentration, which was further confirmed by surface pressure–area isotherms obtained from Langmuir–Blodgett (LB) films (Figure S3 in the Supporting Information). The driving force for this self-assembly process is most likely the presence of many favorable interstrand van der Waals interactions, and the dimensions derived from these DLS and LB experiments suggest that *st*-PEA indeed self-assembles into triple-helix aggregates.

The viscosity increases upon increasing the *st*-PEA concentration and at concentrations above 20 wt % in CHCl₃ *st*-PEA forms an organogel (Figure 11, top), similar to the gelation behavior observed for syndiotactic PMMA polymers.[21] The origin of the formation of this *st*-PEA gel is likely the formation of physical crosslinks, in which a single-helix chain interconnects several different triple-helices as described above (Figures 10 and Figure 11, bottom).

This gel of *st*-PEA (20 wt % in CHCl₃) was further investigated with scanning tunneling microscopy (STM) on a highly-oriented pyrolytic graphite (HOPG) surface (Figure 12). This allowed us to *directly* observe aggregates of *st*-PEA bundles. To prevent drying of the gel, 10 % (v/v) of 1-phenyloctane was added. STM at the gel/solid interface revealed the presence of helix-like arrays of bright ovals. The arrays are 35($\pm$3) Å wide and the distance between their centers is 47($\pm$5) Å. Within an array the bright ovals

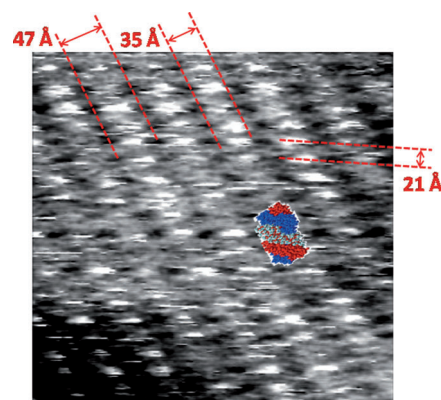

Figure 12. STM topography image of a monolayer of *st*-PEA aggregates at the interface of HOPG and CHCl₃/1-phenyloctane (9:1 v/v); 35× 35 nm², $V_{bias} = -0.280$ V, $I_{set} = 0.5$ pA; structural features of the helix-like arrays are indicated in red and a molecular model of part of a *st*-PEA triple helix is superimposed.

are 21($\pm$5) Å apart. The use of the lowest possible tunneling current in our STM setup ($\sim$0.5 pA) appeared to be essential for successful imaging. Already at this current it appeared very difficult to keep the molecular layer stable, whereas at only slightly higher currents ($\sim$1 pA) the adsorbed arrays were swept away apparently by a physical interaction with the STM tip. This interaction is believed to be the main reason for the far from ideal resolution of the STM image. Since low tunneling currents are directly related to large sample-tip distances, it can be assumed that the observed arrays are several nanometers thick. However, despite the somewhat low resolution, the STM images reveal a characteristic pattern of *st*-PEA bundles, which are clearly much thicker than a *st*-PEA single helix. The dimensions of these bundles correspond well with the *st*-PEA triple-helix structure found with MM/MD simulations. Both the diameter of the triple-helix arrays and the interchain top–top distance between the interconnected single helices in these arrays (observed as bright ovals in the STM image) match perfectly to the model depicted in the bottom part of Figure 9. Hence, it seems that *st*-PEA binds to the graphite surface in its more compact triple-helix conformation (Figure 9, bottom and Figure 12).

The driving force for *st*-PEA to adopt this conformation might well stem from the presence of 1-phenyloctane in the solvent mixture, the hydrophobicity of which forces *st*-PEA to be more compact. It might also be that in this more compact conformation the triple helices simply have a more favorable interaction with the underlying graphite surface, thus providing the driving force for *st*-PEA to adopt this conformation. Note that the STM image represents only a local snapshot of a highly ordered monolayer of *st*-PEA triple helices physisorbed on the graphite surface, and that the physical crosslinks between them in solution, as proposed in Figure 11, are not observed here.

The STM image indicates that the helices are highly aligned at the microscopic level, which is confirmed by the formation of a lyotropic nematic phase at concentrations above 20 wt% in CHCl$_3$ (Figure 13, left).[15]

The presence of crosslinks does not allow us to further increase the wt% of *st*-PEA once a stiff gel is formed. As such the viscosity drop characteristic for LC solutions could not be observed. The maximum concentration depends on

the molecular weight (M_w) of the *st*-PEA polymers (25 wt% for $M_w = 120$ kDa, 35 wt% for $M_w = 24$ kDa and 40 wt% for $M_w = 8$ kDa). These physical crosslinks also hamper formation of highly macroscopically aligned films or fibers from these concentrated LC solutions, since they prevent the helices from flowing. The lack of macroscopic alignment in the nematic phase was confirmed by X-ray diffraction (XRD), which shows formation of long-range ordered structures with a random orientation (Figure 13, right). Some degree of alignment could be achieved by applying shear, but the samples go back to their non-aligned conformation upon releasing the shear pressure.

***st*-PEA aggregates in the solid state and melt**: Experimental proof for the existence of *st*-PEA aggregates in the solid state was obtained by SAXS studies of *st*-PEA at different temperatures (Figure 14). Regardless of the temperature,
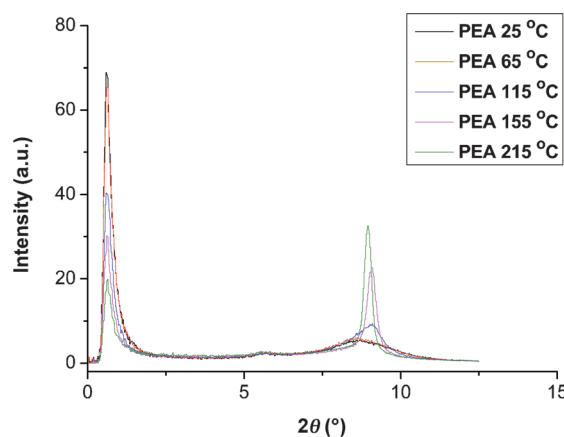

Figure 14. SAXS data of *st*-PEA with $M_w = 120$ kDa at various temperatures.

the pattern shows two characteristic peaks at values for 2θ of 0.60° and 9.36°. The peak at 0.60° corresponds to a periodicity of 145 Å, which roughly matches with the pitch of the triple helix as determined by MM/MD modeling of *st*-PEA (Figure 9, top). This peak seems to reveal a Porod-type behavior, with the intensity being proportional to $1/q$, and is as such representative of worm-like structures, in agreement with the rigid rod-like character of the *st*-PEA triple helix. It should be noted that this peak is very close to the beam stop and that more extensive measurements are required to confirm this. The small angle intensity as such is considerably higher than we normally observe in polymeric samples indicating that indeed long-range, ordered structures are being formed. The peak at 9.36° matches a lattice distance of 9.5 Å, which corresponds to the cross-sectional distance of the single helices in the triple-helix structure (10 Å), which is in agreement with the data reported by Tokita and Shikinaka.[20] *st*-PEA in its solid state was obtained by precipitation from concentrated *st*-PEA solutions in CHCl$_3$ upon addition of MeOH, and as such the observation of these helical aggregates in the solid state further confirms
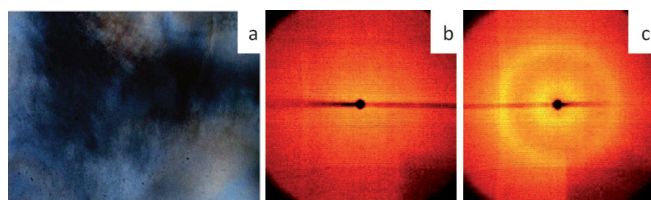

Figure 13. a) Representative polarizing optical micrograph of the texture of *st*-PEA with $M_w = 120$ kDa in solution (CHCl$_3$, 25 °C) showing the formation of a nematic phase. Crossed polarizers, magnification 20×. X-ray diffraction pattern of a *st*-PEA solution ($M_w = 24$ kDa) in CHCl$_3$ at 25 °C at a concentration of: b) 30 wt% or less (isotropic phase), and c) 35 wt% (randomly-oriented nematic phase; right).

the above-described self-assembly behavior of *st*-PEA chains in solution.

Upon heating the sample above the melting transition as observed by differential scanning calorimetry (DSC, $T_m = 105\,°C$ for $M_w = 120$ kDa; vide infra) the peak at 0.60° does not disappear, suggesting that *st*-PEA is still present in its triple-helix form above the T_m. Remarkably, the SAXS peak at 9.36° *sharpens* substantially upon heating the sample (Figure 14), indicating that the *st*-PEA chains (within the triple-helix bundle) form a more ordered structure upon heating above T_m. In order to find an explanation for this effect, we studied the phase behavior of *st*-PEA in more detail.

The behavior of solid *st*-PEA samples upon heating and cooling was studied by differential scanning calorimetry (DSC). Three *st*-PEA samples of different M_w were studied and all show a melting and crystallization transition, with temperatures increasing according to their M_w (Figure 15 and Table 1).
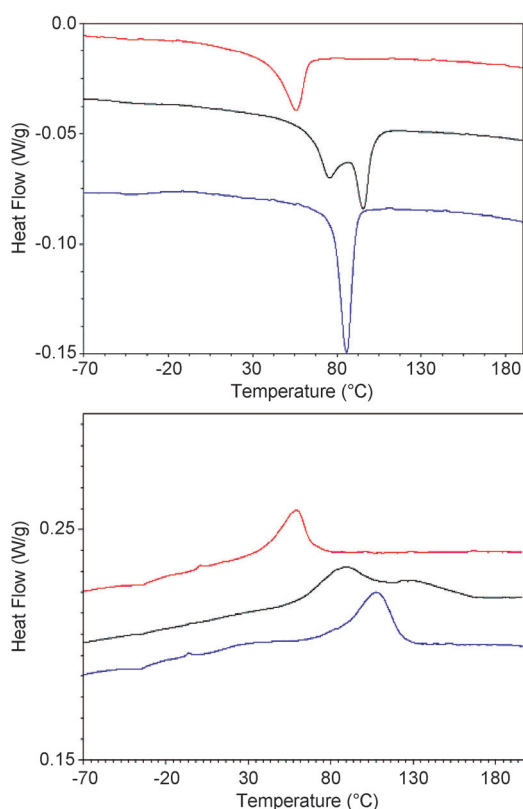
Table 1. Phase-transitions temperatures of *st*-PEA polymers as determined by DSC.

M_w [kDa]	T_m [°C]	T_c [°C]	ΔH_m [J g^{-1}]
120[a]	108	86	21
120[b][15]	150	110	24
24	89, 130	96, 76	25
8	59	56	12

[a] *st*-PEA sample obtained by precipitation from a concentrated CHCl$_3$ solution by addition of MeOH. [b] *st*-PEA sample obtained by slow evaporation of CHCl$_3$.

than slow crystallization by slow evaporation of CHCl$_3$,[17] which allows the formation of a more ordered and thus more favorable polymer packing (less crosslinks). This is emphasized by the observation of two melting and crystallization peaks in the *st*-PEA sample with a M_w of 24 kDa. This polymer sample was obtained by precipitation from concentrated CH$_2$Cl$_2$ solutions upon addition of MeOH. Apparently, the M_w of these polymers and their M_w distribution allow the chains to form two different crystal packings.

Part of the polymers precipitate in a physically cross-linked manner (vide infra), giving rise to lower values of T_m and T_c. These values are in line with those obtained for the other two *st*-PEA samples of different M_w that are crystallized upon addition of MeOH. A second fraction of the polymer sample crystallizes in a more ordered fashion, most likely forming less physical crosslinks, therefore giving rise to higher values for T_m and T_c. Similar effects of crystallization are observed for the other *st*-PEA samples, although only upon changing the sample preparation and thus never in one sample as is the case for *st*-PEA with a M_w of 24 kDa. Surprisingly, the two different crystal packings in this polymer sample are still observed in the second and even third heating and cooling cycle, although the sample has been heated to temperatures well above the T_m in the first heating and cooling cycle. This indicates that the triple helices cannot move freely above the T_m, and thus cannot change their crystal packing or cross-linking behavior.

Above the T_m, *st*-PEA forms a thermotropic nematic phase regardless of the molecular weight (Figure 16). This behavior above the T_m can only be explained by the above-described stability of the (triple helix) aggregate bundles of *st*-PEA, because the individual *st*-PEA chains are much too flexible to form a stable nematic phase (vide supra). These results indicate that the melting transition as observed by DSC can be interpreted as a crystalline-to-nematic transition
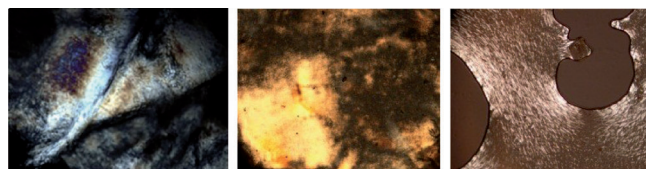

Figure 15. DSC curves (endo up) of *st*-PEA samples with different molecular weights; second cooling curve (top; cooling at $2\,°C\,min^{-1}$) and third heating curve (bottom; heating at $2\,°C\,min^{-1}$ after cooling with $2\,°C\,min^{-1}$). Red lines: 8 kDa; black lines: 24 kDa; blue lines: 120 kDa.

The values for the melting and crystallization temperatures, T_m and T_c, respectively, are further influenced by the crystallization procedure with which the polymers are obtained. Rapid precipitation from concentrated CHCl$_3$ or CH$_2$Cl$_2$ solutions by addition of MeOH yields lower values

Figure 16. Representative polarizing optical micrographs of the textures of *st*-PEA with $M_w = 120$ kDa at 240 °C (left), $M_w = 8$ kDa at 124 °C (middle) and $M_w = 8$ kDa at 260 °C under shear (right) showing the formation of a nematic phase. Crossed polarizers, magnification $10\times$.

FULL PAPER

(K–N). Below the T_m the triple helices apparently form a crystal packing, whereas above the T_m they seem to exist as weakly interacting (albeit still physically crosslinked) rigid-rod bundle-like triple-helical aggregates of *st*-PEA. The melting of these triple-helix crystals is reflected by the temperature profile of the WAXS pattern of *st*-PEA, which shows a broadening of the peaks at higher values of 2θ (from $20° < 2\theta < 40°$) upon heating (Figure 17). This is clear-
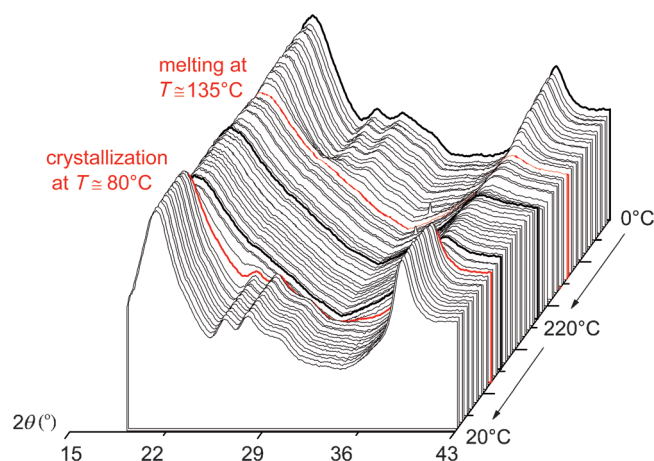

Figure 17. Temperature profile of the WAXS data of *st*-PEA with $M_w = 120$ kDa.

ly indicative for loss of order in the sample, and is thus in agreement with melting of crystals. Upon cooling, the crystal packing is restored. A nematic-to-isotropic transition[15] is observed at about 300 °C, which can be interpreted to be associated with formation of "free" (non-aggregated) *st*-PEA chains in the solid state by dissociation of the triple-helical aggregates. However, this phase transition coincides with the onset of polymer decomposition.

Attempts to obtain highly (macroscopically) aligned samples by melt processing of *st*-PEA in its nematic phase were hampered by the presence of physical crosslinks between the *st*-PEA aggregates, which prevented the material from flowing. Apparently, the interchain van der Waals interactions are strong enough to prevent the individual (single helix) *st*-PEA chains to slide along the axis of the triple helix, hampering the aggregates to move independently. The presence of these physical crosslinks above the T_m was confirmed by rheology measurements (Figure S4 in the Supporting Information).

^{13}C CP-MAS NMR spectroscopy provided further evidence for the solid-state structure of *st*-PEA at different temperatures. Analysis of the carbonyl region of the ^{13}C CP-MAS NMR spectrum of *st*-PEA both at 50 °C and at 170 °C reveals the presence of several spinning side bands, indicated with an asterisk in the spectra (Figure 18). Herzfeld and Berger analysis[25] of the spinning side band intensities of *st*-PEA at 50 °C gives chemical shift tensor values typical for a carbonyl ester group[26] of a powder sample, which is in agreement with the observed solid crystalline phase for *st*-
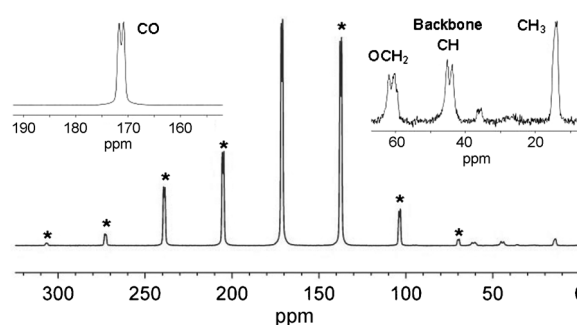
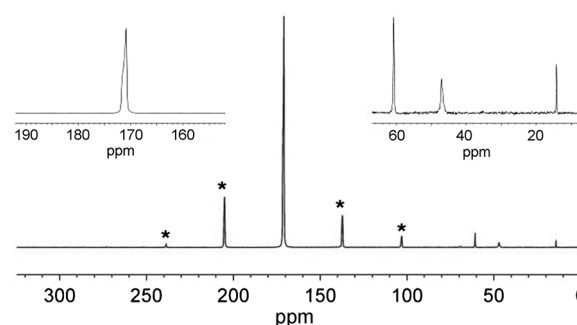Figure 18. ^{13}C CP-MAS NMR spectra (carbonyl region) of *st*-PEA at 50 °C (top: solid phase) and 175 °C (bottom: nematic phase). Spinning sidebands are marked with an asterisk.

PEA. At 170 °C *st*-PEA forms a nematic liquid crystalline (LC) phase. The chemical shift anisotropy values have changed significantly: its asymmetry parameter has changed from 0.34 to 1.0, whereas the anisotropy δ_{ani} has been reduced from 90 to 34 ppm. This can be due to the motion of the carbonyl group and the polymer chains themselves as well as the orientation of the chains in the rotor. In general, when spinning at the magic angle, there is no preferred orientation of the director of a nematic liquid crystal.[27] Hence, the observed change in anisotropy can only be due to restricted motion of the carbonyl groups in the nematic phase. Upon cooling, the original sideband pattern reappears, indicating that the director of the nematic phase does not have a preferred orientation indeed. The change in anisotropy upon heating is linked to the dissociation of the crystalline phase formed by the aggregated *st*-PEA bundles, leading to the formation of what appears to be weakly interacting triple helices in the melt. An isotropic rotation over any axis, be it the H−C−C=O axis or the helix axis, would lead to an anisotropy parameter equal to zero, representative of cylindrical symmetry. This is clearly not the case and a restricted rotation of the ester group about the H−C−C=O axis is a likely scenario. For a restricted rotation between two orientations about this axis that would give an asymmetry parameter of 1, the angle between the two (equally) populated sites should be 134° (or 226°). However, the anisotropy parameter δ_{ani} would only be reduced to 54 ppm, in-

stead of the observed 34 ppm. Liberation of the ester moiety, however, could reduce this anisotropy further.

As reported previously, splitting of the peaks is observed at low temperature (50 °C) as a result of the alternating *syn-syn-anti-anti* configuration of the H−C−C=O torsions (vide supra).[17b] Upon heating, this splitting pattern disappears and the peaks merge into a single one (Figure 18 and Figure 19). This process is reversible, and the peaks split up
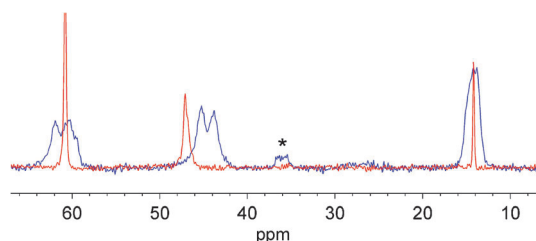

Figure 19. ^{13}C CP-MAS NMR spectrum of *st*-PEA (aliphatic region) at 50 °C (blue) and 175 °C (red). Spinning sidebands are marked with an asterisk.

again upon cooling. This means that the chains undergo rapid reorientations and the signal is representative for the average conformation. Most likely, this reorientation corresponds to rapid *syn–anti* conversions of the H−C−C=O torsions upon heating, which is in agreement with the energies of *st*-PEA polymers in a *syn-syn-anti-anti* and more random conformation that are in a similar range (vide supra). This rotation is possibly due to the melting of the crystal packing of the *st*-PEA (triple helix) aggregates, thus providing more space and rotational freedom for the individual *st*-PEA chains in the molten aggregates. These rotations are also observed in the MD/MM simulations (vide supra). The ^{13}C NMR spectrum of *st*-PEA in solution does not show the above-described splitting, even at concentrations above 5 wt%, indicating that aggregation and formation of the triple helices themselves does not prevent the single helices from having (rotational) mobility in solution. Restricted motion of the H−C−C=O torsion angles in the triple helix is apparently a crystal-packing effect. Remarkable is the downfield shift ($\Delta\delta \sim 2$ ppm) observed for the methine signal of the backbone-carbon atom ($\delta \sim 45$ ppm) upon heating, whereas all other signals retain their original shift (Figure 19). This shift of the backbone-carbon signal is in agreement with the above-described rotational freedom of the single helices upon heating. As a result of the rapid changes in the H−C−C=O torsions, the chemical environment around the backbone carbon atoms apparently changes slightly, resulting in a downfield shift.

The increased rotational freedom of the single helices in the triple-helix structures observed upon heating is most likely also responsible for the sharpening of the peak at 9.36° in the SAXS pattern (Figure 14). Apparently, the single-helix chains in the triple helix adopt a slightly disordered conformation in the crystalline phase in order to allow formation of a tight crystal packing. This disorder is

mainly present in the ethyl groups of the side chains,[17] and is likely governed by steric interactions with neighboring triple helices. Upon heating, the side groups of the single helices gain rotational freedom around the HC−C=O bond, thus providing the space to adopt a more defined structure of the triple helix, thus resulting in a sharpening of the peak in the SAXS pattern.

Comparison of the NMR signals (at 50 °C) before and after heating the sample to 175 °C reveals a sharpening of the peaks after cooling, which is most pronounced in the carbonyl signal (Figure 20). This indicates that the crystal
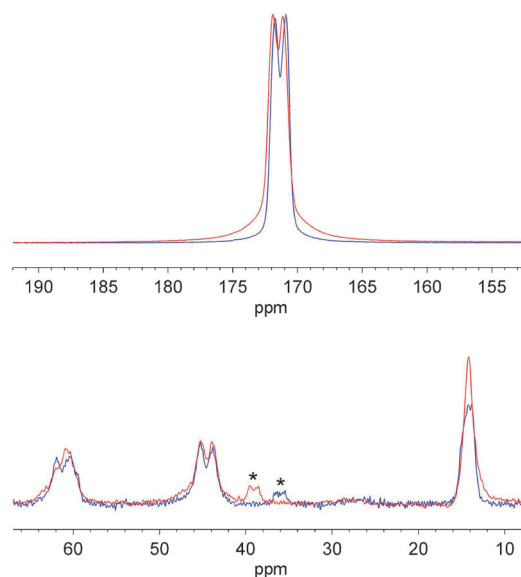

Figure 20. ^{13}C CP-MAS NMR spectra of *st*-PEA at 50 °C before (red) and after (blue) heating to 175 °C. Spinning sidebands are marked with an asterisk.

packing in the solid state is enhanced and the sample has undergone recrystallization during the heating and cooling process. The increased crystallinity of the sample is further emphasized by the decreased intensity of the signal that represents the amorphous fraction of the backbone carbon, which is observed as a broad signal at $\delta = 47.8$ ppm. However, as stated above, the presence of physical crosslinks in the sample prevents the helices from moving and as such prevents the sample from complete recrystallization.

The above-described results strongly suggest that the formation of *st*-PEA triple helices ("tertiary structure") is at the basis of the observed liquid crystalline properties of polycarbenes. The helical ("secondary") structure of the single helices allows too much flexibility. The crosslinks present between several triple helices account for the high modulus of these polymers above the T_m, which is generally considered as beneficial. Unfortunately, the presence of these crosslinks in both the lyotropic and thermotropic nematic phase also hampers flow of the polymers, which is necessary to obtain highly macroscopically aligned structures. However, the results presented here are expected to contribute to

FULL PAPER

the development of suitable processes that allow exploitation of these sp³-based main-chain liquid-crystalline polymers to their full potential.

Conclusion

We have demonstrated through a combination of experimental measurements and computational MM/MD modeling that poly(ethylidene acetate) (*st*-PEA) self-assembles into higher-order aggregates, which explains the thus far poorly understood LC behavior of this polymer. The combined information from molecular mechanics-based molecular dynamic studies (MM/MD), scanning tunneling microscopy (STM), Langmuir–Blodgett surface pressure-area isotherms, WAXS, SAXS and X-ray diffraction studies, DSC, polarized microscopy and solid state NMR spectroscopy strongly suggests that *st*-PEA helices self-assemble into van der Waals-stabilized triple-helix aggregates revealing rigid-rod behavior.

Molecular modeling reveals that *st*-PEA strands, having a fully sp³-based backbone structure, adopt a helical ("secondary") structure due to steric repulsion between their ethyl side groups. Surprisingly, these helices are rather flexible and as such the "secondary structure" of these polymers cannot be held responsible for the observed liquid-crystalline behavior. However, this flexibility also allows the assembly of three of these single *st*-PEA helices into a triple-helical supramolecular ("tertiary") structure, which is stabilized solely by interchain van der Waals interactions. This behavior is rather unique for synthetic polymers. Assembly into these triple-helix structures allows *st*-PEA to reveal rigid, rod-like behavior, and the "tertiary structure" of *st*-PEA dictates its liquid-crystallinity. Formation of higher-order *st*-PEA aggregates is confirmed experimentally. Self-assembly of *st*-PEA occurs readily in solution at concentrations higher than 1 wt % as indicated by detection of rod-like particles with dynamic light scattering (DLS) experiments. Self-assembly of *st*-PEA chains into higher-order rod-like aggregates upon increasing the *st*-PEA concentration was further confirmed by surface pressure–area isotherms obtained from Langmuir–Blodgett (LB) films. The dimensions derived from these DLS and LB experiments suggest that *st*-PEA self-assembles into triple-helix aggregates similar to the MM/MD modeled structures.

At concentrations above 20 wt % the *st*-PEA triple helices form a polymer gel due to physical crosslink formation (single-helix chains interconnecting several different triple helices). The *st*-PEA aggregate bundles could be directly observed in this polymer gel by scanning tunneling microscopy. The dimensions of these bundles correspond well with the *st*-PEA triple-helix structure found with MM/MD simulations. This *st*-PEA gel reveals lyotropic liquid-crystalline behavior, which is not observed at lower *st*-PEA concentrations, thereby emphasizing that the material properties of *st*-PEA are significantly influenced by formation of these assemblies.

st-PEA assemblies are also present in the solid state, which appears to be composed of a crystalline packing of triple-helix aggregates. Upon heating, melting of these rod-like crystals is observed, whereas the individual (triple helix) rod-like bundles stay intact. Above the melting temperature, these rod-like aggregate bundles give rise to the formation of a thermotropic nematic phase, which is stable up to 300 °C. At even higher temperatures a nematic-to-isotropic transition is observed, indicating that the aggregates start to disassemble into individual flexible *st*-PEA chains. These results emphasize the strong influence of *st*-PEA self-assembly on the polymer properties.

The presence of physical crosslinks after assembly of *st*-PEA into its "tertiary structure" gives rise to a rather high modulus for these polymers, which is retained above the LC melting point. This makes *st*-PEA potentially interesting for structural applications. The disadvantage of these crosslinks is that the material exhibits very limited flow in both its lyotropic and thermotropic nematic phase, which makes it more difficult to process this material or to obtain macroscopically aligned *st*-PEA films and fibers. Further research is necessary to improve the processing ability of these new liquid-crystalline materials in order to exploit them to their full potential.

The results described here emphasize the potential of the formation of helical assemblies for obtaining novel materials with unexpected properties dictated by their "tertiary structure". This behavior bears some similarities with the effects of the secondary and tertiary structure of biological macromolecules (e.g., proteins, DNA) on their material properties and biochemical function.

Experimental Section

st-PEA samples of different molecular weight were obtained according to known procedures.[17] Solvents were used without further purification.

Computational methods: The classical molecular dynamics simulations were performed with our in-house software CM3D, using the amber gaff force field. Atomic (RESP) charges were obtained by matching the electrostatic potential around an optimized structure of a monomer unit (CH₃−CHC(O)OC₂H₅−CH₃) to a reference potential obtained from a Hartree–Fock/6-31G electronic structure calculation, following the amber force field protocol. We adapted the HCCO torsion potentials of the amber force field to match the free energy barrier for side-chain rotation to a reference potential. This reference potential was obtained at the density functional theory (PBE+VdW/TZVP) level of theory by performing a series of constrained molecular dynamics simulations with the CP2K program to obtain the free energy of rotation. A series of polymer chains were built from the optimized monomer structure by applying simple translation, rotation and inversion rules. By changing the angle of rotation for each subsequent monomer in the chain, left- and right-handed backbone chains were generated. Also, the initial side-chain orientations were varied between all *syn*, all *anti*, as well as several alternating patterns. These structures were energy minimized and simulated for 1 ns in the NVT ensemble at temperatures of 5, 100, 300, 400, 500, and 600 K. A Nose–Hoover chain was used to maintain the temperature. To find the most stable structures, we also performed annealing simulations, in which the velocities were slowly scaled back to zero Kelvin during a 1 ns simulation. The position trajectories were stored for analysis.

Dynamic light scattering: DLS measurements were performed on a Malvern Zetasizer Nano ZS.

Polarizing optical microscopy (POM): A Leica DMLD polarizing optical microscope equipped with a Linkam hot-stage or a Nikon Eclipse E600 polarizing optical microscope equipped with a Nikon DSLR:1 camera was used. The thermotropic behavior was studied between untreated glass slides by using heating and cooling rates of 10 °C min^{-1}. The lyotropic behavior was investigated by using solutions of *st*-PEA in CH$_2$Cl$_2$ at different wt % at 25 °C.

X-ray diffraction: XRD data were recorded on a Bruker AXS D8 Discover X-ray diffractometer with a Hi-Star 2D detector by using Cu$_{K\alpha}$ radiation filtered by cross-coupled Göbbel mirrors at 40 kV and 40 mA.

Differential scanning calorimetry: A DSC Q1000 of TA-Instruments in the modulated mode was used. The heating and cooling rate were 2 °C min^{-1}, the amplitude of temperature modulation was 0.5 °C and the period of modulation 60 s. The T_m and T_c values were determined from the heat flow curves.

Rheology measurements: A Rheometric SR 5000 controlled stress rheometer using parallel plates with a diameter of 25 mm was employed. A strain sweep was performed to confirm the linear viscoelastic region of the samples, followed by a frequency sweep.

Simultaneous small-angle X-ray scattering (SAXS) and wide angle X-ray scattering (WAXS): Measurements were performed at the Dutch–Belgian beam-line (DUBBLE) at ESRF in Grenoble, France. The sample detector distance was about 2 m, whereas the X-ray wavelength was 1.24 Å ($E = 10$ keV). The scattering vector q is defined as $q = (4\pi/\lambda)\sin\theta$, where $\sin\theta$ is half of the scattering angle. A Linkam hot stage was used for heating–cooling and was performed at a rate of 10 °C min^{-1}.

^{13}C CP-MAS NMR spectroscopy: Spectra were recorded on a Chemagnetics CMX 600 MHz NMR spectrometer. An HX double resonant 3.2 mm pencil design Chemagnetics probe was used, tuned to 599.995 MHz for protons and 150.872 MHz for carbon. Cross polarization was performed with a 2 ms contact time and rf-field strengths on proton and carbon of 50 and 55 kHz, respectively, and a 5 kHz linear ramp on carbon. Magic angle spinning at speeds of 5 kHz was used and proton decoupling with an optimized CM sequence[28] (8° phase excursion, 10.8 µs pulse width) at an rf-field strength of 92 kHz was employed during acquisition.

Scanning tunneling microscopy: STM was performed in the constant current mode by using a home-built STM setup.[24] Tips were mechanically cut from 0.5 mm diameter Pt$_{0.8}$Ir$_{0.2}$ wire and freshly cleaved ZYB-grade HOPG (NT-MDT) was used as substrate. All measurements were performed at solid/liquid interfaces created by the application of a droplet of the solution under investigation between the tip and the substrate. The piezo element of the STM was calibrated in situ by lowering the bias voltage to 100 mV and raising the tunneling current to 50 pA, which allowed imaging of the HOPG surface underneath the molecules. Raw STM data were processed only by the application of background flattening.

Pressure–area isotherms: Measurements were recorded by using a KSV Minitrough (KSV Instruments, Ltd.) with a surface area of 243.06 cm^{-2}, equipped with a Lauda RM6 cooling system at a temperature of 25 °C. An aliquot (35 µL) of a solution of *st*-PEA in CHCl$_3$ at a concentration of 1.02 mg mL^{-1} was placed on a water surface and allowed to spread evenly over 15 min. The pressure–area isotherm was collected at a 10 mm min^{-1}.

Acknowledgements

[1] Y. Furusho, E. Yashima, *J. Polym. Sci. Part A* **2009**, *47*, 5195.

[2] G. Felsenfeld, D. R. Davies, A. Rich, *J. Am. Chem. Soc.* **1957**, *79*, 2023.

[3] *Triple Helix Forming Oligonucleotides* (Eds.: C. Malvy, A. Harel-Bellan, L. L. Pritchard), Kluwer, Norwell, **1999**, p. 307.

[4] F. A. Buske, J. S. Mattick, T. L. Bailey, *RNA Biol.* **2011**, *8*, 427.

[5] R. D. Harkness, *Biol. Rev.* **1961**, *36*, 399.

[6] A. E. Rowan, R. J. M. Nolte, *Angew. Chem.* **1998**, *110*, 65; *Angew. Chem. Int. Ed.* **1998**, *37*, 63.

[7] J. J. L. M. Cornelissen, A. E. Rowan, R. J. M. Nolte, N. A. J. Sommerdijk, *Chem. Rev.* **2001**, *101*, 4039.

[8] E. Yashima, K. Maeda, H. Iida, Y. Furusho, K. Nagai, *Chem. Rev.* **2009**, *109*, 6102.

[9] a) J. Kumaki, T. Kawauchi, K. Okoshi, H. Kusanagi, E. Yashima, *Angew. Chem.* **2007**, *119*, 5444; *Angew. Chem. Int. Ed.* **2007**, *46*, 5348; earlier reports described the stereocomplex as a 1:1 double helix: b) E. Schomaker, G. Challa, *Macromolecules* **1989**, *22*, 3337.

[10] T. Kawauchi, A. Kitaura, J. Kumaki, H. Kusanagi, E. Yashima, *J. Am. Chem. Soc.* **2008**, *130*, 11889.

[11] T. Serizawa, K. Hamada, T. Kitayama, N. Fujimoto, K. Hatada, M. Akashi, *J. Am. Chem. Soc.* **2000**, *122*, 1891.

[12] J. P. Kennedy, J. L. Price, K. Koshimura, *Macromolecules* **1991**, *24*, 6567.

[13] G. Ungar, *Macromolecules* **1986**, *19*, 1317.

[14] L. Li, W. H. de Jeu, *Phys. Rev. Lett.* **2004**, *92*, 075506.

[15] L. Li, W. H. de Jeu, *Macromolecules* **2003**, *36*, 4862.

[16] a) E. Jellema, A. L. Jongerius, J. N. H. Reek, B. de Bruin, *Chem. Soc. Rev.* **2010**, *39*, 1706; b) E. Ihara, *Adv. Polym. Sci.* **2010**, *231*, 191; c) N. M. G. Franssen, A. J. C. Walters, J. N. H. Reek, B. de Bruin, *Catal. Sci. Technol.* **2011**, *1*, 153; d) N. M. G. Franssen, J. N. H. Reek, B. de Bruin, *Chem. Soc. Rev.* **2013**, *42*, 5809.

[17] a) E. Jellema, A. L. Jongerius, G. Alberda van Ekenstein, S. D. Mookhoek, T. J. Dingemans, E. M. Reingruber, A. Chojnacka, P. J. Schoenmakers, R. Sprenkels, E. R. H. van Eck, J. N. H. Reek, B. de Bruin, *Macromolecules* **2010**, *43*, 8892; b) D. G. H. Hetterscheid, C. Hendriksen, W. I. Dzik, J. M. M. Smits, E. R. H. van Eck, A. E. Rowan, V. Busico, M. Vacatello, V. Van Axel Castelli, A. Segre, E. Jellema, T. G. Bloemberg, B. de Bruin, *J. Am. Chem. Soc.* **2006**, *128*, 9746; c) E. Jellema, P. H. M. Budzelaar, J. N. H. Reek, B. de Bruin, *J. Am. Chem. Soc.* **2007**, *129*, 11631; d) E. Jellema, A. L. Jongerius, A. J. C. Walters, J. M. M. Smits, J. N. H. Reek, B. de Bruin, *Organometallics* **2010**, *29*, 2823; e) M. Rubio, E. Jellema, M. A. Siegler, A. L. Spek, J. N. H. Reek, B. de Bruin, *Dalton Trans.* **2009**, 8970; f) A. J. C. Walters, E. Jellema, M. Finger, P. Aarnoutse, J. M. M. Smits, J. N. H. Reek, B. de Bruin, *ACS Catal.* **2012**, *2*, 246; g) A. J. C. Walters, O. Troeppner, I. Ivanović-Burmazović, C. Tejel, M. P. del Río, J. N. H. Reek, B. de Bruin, *Angew. Chem.* **2012**, *124*, 5247; *Angew. Chem. Int. Ed.* **2012**, *51*, 5157; h) N. M. G. Franssen, K. Remerie, T. Macko, J. N. H. Reek, B. de Bruin, *Macromolecules* **2012**, *45*, 3711; i) N. M. G. Franssen, J. N. H. Reek, B. de Bruin, *Dalton Trans.* **2013**, *42*, 9058; j) N. M. G. Franssen, B. de Bruin, E. Jellema, A. L. Jongerius, PCT Int. Pat. Appl. WO 2011/157444A1, **2011**; k) B. Bantu, K. Wurst, M. R. Buchmeiser, *J. Organomet. Chem.* **2007**, *692*, 5272.

[18] a) E. Ihara, N. Haida, M. Iio, K. Inoue, *Macromolecules* **2003**, *36*, 36; b) E. Ihara, M. Fujioka, N. Haida, T. Itoh, K. Inoue, *Macromolecules* **2005**, *38*, 2101; c) E. Ihara, M. Kida, M. Fujioka, N. Haida, T. Itoh, K. Inoue, *J. Polym. Sci. Part A* **2007**, *45*, 1536; d) E. Ihara, T. Hiraren, T. Itoh, K. Inoue, *J. Polym. Sci. Part A* **2008**, *46*, 1638; e) E. Ihara, T. Hiraren, T. Itoh, K. Inoue, *Polym. J.* **2008**, *40*, 1094; f) E.

Ihara, Y. Goto, T. Itoh, K. Inoue, *Polym. J.* **2009**, *41*, 1117; g) E. Ihara, Y. Ishiguro, N. Yoshida, T. Hiraren, T. Itoh, K. Inoue, *Macromolecules* **2009**, *42*, 8608; h) E. Ihara, K. Saiki, Y. Goto, T. Itoh, K. Inoue, *Macromolecules* **2010**, *43*, 4589; i) E. Ihara, H. Takahashi, M. Akazawa, T. Itoh, K. Inoue, *Macromolecules* **2011**, *44*, 3287; j) E. Ihara, Y. Hara, T. Itoh, K. Inoue, *Macromolecules* **2011**, *44*, 5955; k) N. M. G. Franssen, J. N. H. Reek, B. de Bruin, *Polym. Chem.* **2011**, *2*, 422.

[19] T. Otsu, T. Yasuhara, K. Shiraishi, S. Mori, *Polym. Bull.* **1984**, *12*, 449.

[20] M. Tokita, K. Shikinaka, T. Hoshino, K. Fujii, J. Mikami, N. Koshimizu, K. Sakajiri, S. Kang, J. Watanabe, K. Shigehara, *Polymer* **2013**, *54*, 995.

[21] J. Spěváček, B. Schneider, *Adv. Colloid Interface Sci.* **1987**, *27*, 81.

[22] Y. Chatani, T. Kobatake, H. Tadokoro, R. Tanaka, *Macromolecules* **1982**, *15*, 170.

[23] M. D. Shoulders, R. T. Raines, *Annu. Rev. Biochem.* **2009**, *78*, 929.

[24] B. Hulsken, R. van Hameren, J. W. Gerritsen, T. Khoury, P. Thordarson, M. J. Crossley, A. E. Rowan, R. J. M. Nolte, J. A. A. W. Elemans, S. Speller, *Nat. Nanotechnol.* **2007**, *2*, 285.

[25] J. Herzfeld, A. E. Berger, *J. Chem. Phys.* **1980**, *73*, 6021.

[26] a) W. S. Veeman, *Prog. Nucl. Magn. Reson. Spectrosc.* **1984**, *16*, 193; b) B. A. Cornell, *J. Chem. Phys.* **1986**, *85*, 4199.

[27] J. Courtieu, D. W. Alderman, D. M. Grant, J. P. Bayles, *J. Chem. Phys.* **1982**, *77*, 723.

[28] G. De Paëpe, B. Eléna, L. Emsley, *J. Chem. Phys.* **2004**, *121*, 3165.